

Superposition of electron-hole density gratings in GaAs generated by quantum control of charge densities and charge currents

Y. Kerachian and H. M. van Driel*

Department of Physics and Institute for Optical Sciences, University of Toronto, Toronto, Ontario, Canada, M5S1A7

Arthur L. Smirl

Laboratory for Photonics and Quantum Electronics, 138 IATL, University of Iowa, Iowa City, Iowa 52242, USA

(Received 21 July 2006; revised manuscript received 9 January 2007; published 19 March 2007)

Quantum interference of single-photon and two-photon absorption of 775 and 1550 nm, ~ 150 fs optical pulses in GaAs at 300 K is known to lead to coherent control of electron-hole pair density and charge currents with the magnitude controlled by the pulses' relative phase and polarization. When the pulses are noncollinearly incident on a (001) GaAs crystal, the relative phase between the pulses varies in the plane of the surface, resulting in current and density gratings. The current grating also produces a charge-neutral electron-hole pair density grating following the completion of dielectric relaxation by the end of the pulses. The two types of density gratings, which are monitored using 830 nm, 150 fs pulses and which decay by ambipolar diffusion and recombination on a 15 ps time scale, are studied as a function of sample azimuthal orientation and pulse polarization. For those polarizations where both density gratings are simultaneously generated, the amplitude of the current-induced density grating is comparable to that of the directly deposited grating and independent of grating period, although the former is related to a third-order optical process and the latter to a second-order process. Superposition and interference of the density gratings are therefore observed, as shown from the azimuthal dependence of the diffraction efficiency.

DOI: [10.1103/PhysRevB.75.125206](https://doi.org/10.1103/PhysRevB.75.125206)

PACS number(s): 78.47.+p, 72.20.Ht, 42.65.-k

I. INTRODUCTION

The control of carrier density and charge currents in semiconductors is both fundamentally and technologically important. While electronic methods are often used to achieve control, it has been shown that optical techniques, and, in particular, quantum interference between absorption pathways of optical beams, can be used without the need of external bias to generate and control pure charge currents,¹⁻⁵ pure spin currents,⁶⁻¹¹ spin-polarized charge currents,¹²⁻¹⁵ as well as carrier¹⁶ and spin densities.¹⁷ Requiring no external bias fields or electrical contacts (and associated deleterious capacitance or inductance effects), the optically generated currents can be produced on a time scale limited by the pulse duration and in locations and areas dictated by the pulse focal properties. For example, in bulk GaAs at 300 K, carrier density and currents were controlled using interference between single- and two-photon absorption processes for phase-related 775 and 1550 nm, ~ 150 fs pulses.^{3,16} The pulses were collinearly incident on the crystal with their relative phase controlled by varying the time delay between the pulses. However, recently we have shown that if orthogonally polarized pulses are noncollinearly incident on GaAs, spin current gratings¹⁸ are produced allowing one to obtain information about the spin spatiotemporal dynamics. We have subsequently shown¹⁹ that one can also produce charge current gratings through quantum interference; because of warping or nonparabolicity of the hole band, a charge-neutral electron-hole population grating (hereafter simply referred to as a pair grating) is formed once dielectric relaxation is complete by the end of the pulses. The pair grating subsequently decays via recombination and ambipolar diffusion.

Charge current generation by quantum interference control (QUIC) can also be understood at the macroscopic level

as being governed by a $\chi^{(3)}$ nonlinear optical process and can therefore occur in centrosymmetric or noncentrosymmetric materials.³ With harmonically related beams, it is also possible to coherently control electron-hole density¹⁶ in a noncentrosymmetric material such as GaAs; at the macroscopic level, this effect can be understood as a $\chi^{(2)}$ process. Hence, it should also be possible to directly inject a pair grating via a $\chi^{(2)}$ process if noncollinearly propagating beams are used.

In this paper, we experimentally demonstrate the production of pair gratings using a $\chi^{(2)}$ process for a (001) oriented sample of GaAs using noncollinearly incident 775 and 1550 nm optical pulses. For certain polarizations of the pump beams, this grating is superposed on, and interferes with, a pair grating, which remains following current generation by a $\chi^{(3)}$ process. Surprisingly, the amplitude (density modulation) of the gratings differs by less than an order of magnitude despite the very different processes used to form them. The ratio of the grating amplitudes is also independent of angle of incidence of the beams (or grating wave vector) and pump pulse intensities.

The remainder of this paper is organized as follows. In the following section, we show how quantum interference in absorption pathways of two harmonically related pulses can induce carrier density and current gratings in a semiconductor. On the basis of earlier work¹⁹ that describes how a current grating can produce a pair grating, we show how the current-generated pair grating can interfere with the one formed directly by carrier density control. In Sec. III, we outline aspects of the experiments, while Sec. IV presents the experimental results and their comparison with a simple model. Finally, we summarize the main findings.

II. THEORETICAL BACKGROUND

A. Pair grating formation via second-order nonlinearity

We consider quantum interference control of carrier density when two noncollinearly propagating optical pulses with carrier frequencies ω and 2ω are simultaneously incident on a semiconductor crystal. Their complex optical electric fields inside the crystal can be written as

$$\mathbf{E}_\omega(\mathbf{r}, t) = E_\omega(t) \hat{\mathbf{e}}_\omega \exp[i(-\omega t + \mathbf{k}_\omega \cdot \mathbf{r} + \phi_\omega)],$$

$$\mathbf{E}_{2\omega}(\mathbf{r}, t) = E_{2\omega}(t) \hat{\mathbf{e}}_{2\omega} \exp[i(-2\omega t + \mathbf{k}_{2\omega} \cdot \mathbf{r} + \phi_{2\omega})], \quad (1)$$

where $\mathbf{k}_{\omega, 2\omega}$, $\hat{\mathbf{e}}_{\omega, 2\omega}$, and $E_{\omega, 2\omega}(t)$ are the propagation vectors, polarization vectors, and field envelopes, respectively, of the ω and 2ω pulses whose phases are given by $\phi_{\omega, 2\omega}$. If the frequencies are chosen such that $\hbar\omega < E_g < 2\hbar\omega$, where E_g is the semiconductor fundamental energy gap, the absorption of the pump pulses leads to a pair density generation at a rate¹⁶

$$\dot{N} = \dot{N}_\omega + \dot{N}_{2\omega} + \dot{N}_I, \quad (2)$$

where $\dot{N}_{2\omega}$ and \dot{N}_ω are the generation rates by one- and two-photon absorptions, respectively, by the 2ω and ω pulses acting independently and \dot{N}_I is the generation rate due to quantum interference between the two absorption processes. For simplicity, in what follows we consider the sample to be optically thin so that we can ignore dispersion effects while taking absorption to occur uniformly throughout the semiconductor thickness and lateral extent; this allows for a one-dimensional description. The interference term in Eq. (2) is then dominated by interference in absorption pathways with negligible contributions from parametric up-conversion of ω photons^{16,17} followed by absorption of 2ω photons. In terms of the linear and nonlinear optical susceptibilities $\tilde{\chi}^{(n)}$, Eq. (2) can be written as¹⁶

$$\dot{N}_{2\omega} = 2\varepsilon_0 \hbar^{-1} \text{Im}[\tilde{\chi}^{(1)}(-2\omega; 2\omega)]:E_{2\omega} \mathbf{E}_{2\omega}^* = (2\hbar\omega)^{-1} \alpha_p I^{2\omega},$$

$$\begin{aligned} \dot{N}_\omega &= 6\varepsilon_0 \hbar^{-1} \text{Im}[\tilde{\chi}^{(3)}(-\omega; \omega, -\omega, \omega)]:E_\omega \mathbf{E}_\omega^* E_\omega \mathbf{E}_\omega^* \\ &= (2\hbar\omega)^{-1} \beta (I^\omega)^2, \end{aligned}$$

$$\dot{N}_I = 4\varepsilon_0 \hbar^{-1} \text{Im}[\tilde{\chi}^{(2)}(-2\omega; \omega, \omega)]:\text{Re}[E_\omega \mathbf{E}_\omega \mathbf{E}_{2\omega}^*]. \quad (3)$$

Here, $I^{2\omega}$ and I^ω are the intensities of the 2ω and ω beams inside the crystal and α_p is the single-photon absorption coefficient. For the zinc-blende semiconductor GaAs with T_d symmetry, $\tilde{\chi}^{(1)}$ has only one unique nonzero element in a principal axis system, and the absorption coefficient for 775 nm is^{20,21} $\alpha_p \sim 1.4 \times 10^6 \text{ m}^{-1}$. The $\tilde{\chi}^{(3)}$ tensor associated with the degenerate two-photon absorption has three distinguishable, nonzero elements, which can be related to the two-photon absorption coefficient β . For a linearly polarized beam incident on (001) GaAs,²² $\beta = \beta_0 [1 + 0.25 \sin^2(2\varphi)]$, where φ is the angle between the beam polarization and the [100] direction and $\beta_0 \sim 10 \text{ cm GW}^{-1}$ for 1550 nm. For the interference term, the $\tilde{\chi}^{(2)}$ tensor has one distinguishable, nonzero element, $\chi_{abc}^{(2)}$, where a , b , and c are different principal crystal axes. For given beam polarizations and sample

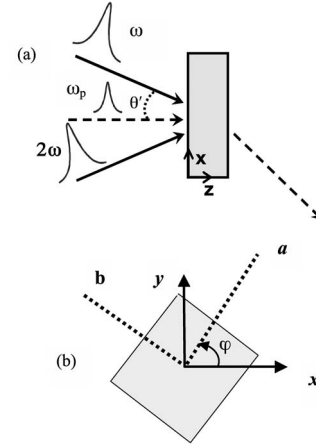


FIG. 1. (a) Geometry for producing a transient population grating by quantum interference control using pump pulses with frequencies ω and 2ω and for monitoring the grating formation and decay by detecting the diffracted probe with frequency ω_p . (b) Semiconductor and beam coordinate system with φ measured from the x axis (solid line) to the principal axis a .

orientation, the degree of control of the carrier density, expressed by the ratio $\dot{N}_I/(\dot{N}_\omega + \dot{N}_{2\omega})$, is largest under balanced conditions, whereby an equal density of carriers is generated by single- and two-photon absorption. This ratio has values of the order of¹⁶ 0.1.

Figure 1 illustrates the geometry used to generate pair gratings in the experiments with pump beams incident in a noncollinear geometry on a (001) surface of GaAs; the z axis is defined to be along the [001] direction with x axis lying in the plane of incidence. If the two pump pulses' propagation vectors make an angle of $\pm\theta$ with the z direction inside the crystal, they can be written as $\mathbf{k}_{\omega, 2\omega} = |\mathbf{k}_{\omega, 2\omega}|(\mp \hat{x} \sin \theta + \hat{z} \cos \theta)$. An s -polarized beam then has $\hat{\mathbf{e}}_{\omega, 2\omega} = \hat{\mathbf{y}}$, and a p -polarized beam has $\hat{\mathbf{e}}_{\omega, 2\omega} = \hat{x} \cos \theta \pm \hat{z} \sin \theta$. We consider only linearly polarized pump pulses which are copolarized or orthogonally polarized with the polarization pairs of the two pump beams denoted by $\mu\nu = pp, ps, sp,$ or ss , where the first and second letters refer to the polarization of ω and 2ω optical pulses, respectively. For small θ , $\cos \theta \approx 1$, and if we define $\xi = -2\varepsilon_0 \hbar^{-1} \text{Im} \chi_{abc}^{(2)} \sin \theta (E_\omega(t))^2 E_{2\omega}(t)$ for each $\mu\nu$, Eq. (3) yields a pair grating generation rate of the form $N_I^{\mu\nu} \cos(K_g x)$ with

$$\dot{N}_I^{pp} = \xi \sin 2\varphi, \quad (4)$$

$$\dot{N}_I^{ps} = -2\xi \cos 2\varphi, \quad (5)$$

$$\dot{N}_I^{sp} = \xi \sin 2\varphi, \quad (6)$$

$$\dot{N}_I^{ss} \equiv 0, \quad (7)$$

where $K_g = 2\pi/\Lambda_g = (2k_\omega + k_{2\omega}) \sin \theta$ is the wave vector for a grating with period Λ_g . The origin of the x axis is chosen to eliminate the constant phase terms indicated in Eq. (1). The $\sin \theta$ term in ξ arises from the z component of one of the

incident fields inside the semiconductor. Note that $\xi=0$ for normally incident beams, and hence there would be no population control for beams normally incident on a (100) surface as discussed previously.¹⁶ For each $\mu\nu$, $N_I^{\mu\nu}$ is obtained from time integration of the above equations. A pair grating is expected to decay via carrier recombination and ambipolar diffusion on a time scale $\gg 1$ ps.

B. Pair grating formation via third-order nonlinearity

As shown elsewhere,¹⁹ it is also possible for the noncollinear beam configuration to produce a charge current grating. In general, the rate of current density injection is given by

$$\dot{J}(\mathbf{r}, t) = \vec{\eta}:E_\omega(\mathbf{r}, t)E_\omega(\mathbf{r}, t)E_{2\omega}^*(\mathbf{r}, t) + \text{c.c.}, \quad (8)$$

where $\vec{\eta}$ is the current injection tensor, which can be written as the sum of three component tensors $\vec{\eta}_c$ related to contributions from electrons ($c=e$), heavy holes ($c=hh$) and light holes ($c=lh$). These tensors are purely imaginary²³ in the independent-particle approximation and are related to a doubly divergent part³ of $\chi^{(3)}(0; \omega, \omega, -2\omega)$. For a semiconductor with zinc-blende symmetry, the tensors have three distinguishable nonzero components, η_c^{aaaa} , η_c^{abba} , and $\eta_c^{aabb} = \eta_c^{abab}$, and those defined by permutations of a , b , and c . Real, coordinate-free current injection factors can be defined²⁴ by $\eta_c^{B1} = -2i\eta_c^{aabb}$, $\eta_c^{B2} = -i\eta_c^{abba}$, and $\eta_c^C = 2i\eta_c^{aabb} + i\eta_c^{abba} - i\eta_c^{aaaa}$. For each $\mu\nu$ and ϕ , the current injection rate along \hat{x} establishes a grating of the form $J_x^{\mu\nu} \sin(K_g x)$, where

$$J_x^{pp} = 2F[\eta^{B1} + \eta^{B2} + \eta^C - (1/2)\eta^C \sin^2(2\phi)], \quad (9)$$

$$J_x^{ps} = \frac{1}{2}F\eta^C \sin(4\phi), \quad (10)$$

$$J_x^{sp} = 2F[\eta^{B2} + (1/2)\eta^C \sin^2(2\phi)], \quad (11)$$

$$J_x^{ss} = -\frac{1}{2}F\eta^C \sin(4\phi). \quad (12)$$

Here, $F = (E_\omega(t))^2 E_{2\omega}(t)$ and we have again used $\cos \theta \approx 1$. The calculated values of the current tensor components for GaAs can be obtained from Ref. 24 for $(2\hbar\omega - E_g) = 180$ meV, appropriate for the experiments described below.

We earlier¹⁹ described how the charge current grating generated by ultrashort pulse produce a transient carrier density and temperature grating. Although the temperature grating decays within 500 fs, the charge grating evolves into a pair grating after dielectric relaxation is complete (typically by the end of the pumping process for a carrier density of $\sim 10^{17}$ cm⁻³). The pair grating has the form $N_I^{\mu\nu} \cos(K_g x)$, where

$$N_I^{\mu\nu} \approx -K_g N^{inj} P^{inj} \tau_{hh} (m_{hh}^*)^{-1}. \quad (13)$$

Here, N^{inj} is the injected electron or hole density and $P^{inj} = (m_{hh}^* u_{hh}^s + m_{\Gamma}^* u_{\Gamma}^s)$ is a measure of the warping of the heavy-hole band with $m_{\Gamma, hh}^*$ being the mobility effective mass for

heavy holes (hh) or Γ -valley electrons; $u_c^s = \mp e^{-1} J_c^{\mu\nu} / [N^{inj} \sin(K_g x)]$ is the swarm or average velocity of the injected carriers ($-$ sign for electrons, $+$ sign for holes) for a given $\mu\nu$, and τ_{hh} is the heavy-hole momentum relaxation time. From the tensor elements and the (density dependent) hole momentum relaxation time,^{20,21} one can calculate the swarm speeds and¹⁹ P^{inj} for a given $\mu\nu$ and hence the amplitude of a pair grating. The pair grating can also be reinforced by the effects related to transfer of electrons between Γ and (X, L) valleys.

C. Interference of pair gratings

For polarization combinations whereby both $N_I^{\mu\nu}$ and $N_I^{\nu\mu}$ are nonzero, the density modulation amplitudes are $\propto \sin \theta \int_{\text{pump}} [E_\omega(t)]^2 E_{2\omega}(t) dt$, so that the ratio $N_I^{\mu\nu} / N_I^{\nu\mu}$ is independent of the pump pulses' intensity and temporal characteristics as well as angle θ . For appropriate GaAs optical and electronic parameters^{20,21} and for¹⁶ $\text{Im}(\chi_{abc}^{(2)}) \sim 6 \times 10^{-11}$ mV⁻¹, we estimate ($\mu\nu \neq ss, ps$) $N_I^{\mu\nu} / N_I^{\nu\mu} \approx 0.5$, surprisingly close to unity given the nature of the different grating generation processes and the underlying microscopic mechanisms leading to them. The ratio of the directly deposited pair grating amplitude to that of the injected carrier density, viz., $|N_I^{\mu\nu} / N_e^{inj}|$, depends on the relative number of carriers injected by single- and two-photon absorptions and $\mu\nu$. Under balance conditions,²⁵ for pp polarization, this ratio is $[2\omega \text{Im}(\chi_{abc}^{(2)}) / (2\varepsilon_0 c n_\omega^2 n_{2\omega})^{3/2} \sqrt{\alpha_p \beta}] \sin \theta$, where $n_{\omega, 2\omega}$ is a refractive index and ε_0 is the vacuum dielectric constant. For GaAs excited by 1550 and 775 nm pulses with $\theta \approx 3^\circ$, we estimate $|N_I^{pp} / N_e^{inj}| \approx 10^{-3}$.

By the end of the pump pulses, for a particular $\mu\nu$ and ϕ , the spatial dependence of the pair population is given by

$$N^{\mu\nu}(x) = N_e^{inj} + [N_I^{\mu\nu} + N_I^{\nu\mu}] \cos(K_g x), \quad (14)$$

where the implicit ϕ dependence is given by Eqs. (4)–(7) and (9)–(12). The pair grating can be detected using diffraction of a probe pulse. The interband absorption coefficient for a probe beam can be expressed²⁶ as $\alpha = \sum_v \alpha_v [1 - f_e(E_v) - f_h(E_v)]$, where the summation is over heavy- and light-hole valence bands ($v=hh, lh$) from which electrons can be excited and $f_{e,h}(E_v)$ are the Fermi occupancy factors evaluated at the appropriate electron or hole energies for the states optically coupled by the probe beam. For GaAs,²⁷ $\alpha_{hh} \approx \frac{2}{3}\alpha_0$ and $\alpha_{lh} \approx \frac{1}{3}\alpha_0$, where²¹ $\alpha_0 = 0.9 \times 10^6$ m⁻¹ is the quiescent absorption coefficient at 830 nm. The probe pulse Pauli blocking factors are dominated²⁷ by $f_e(E_{lh})$. As shown earlier,¹⁹ a first-order carrier density grating produces a grating in $f_{e,h}$ and hence a grating in the probe absorption coefficient with amplitude $\Delta\alpha$ and the refractive index Δn obtained through a Kramers-Kronig analysis.²⁵ One then has that the diffraction efficiency (diffracted intensity divided by incident intensity) of the (thin) grating in first order is²⁸ $\zeta = e^{-\alpha_0 L} (L^2/4) [(k_p \Delta n)^2 + (\Delta\alpha/2)^2]$, where k_p is the probe vacuum propagation constant and L is the thickness of the optically thin crystal. For conditions corresponding to our experimental situation, calculations indicate that the index grating is much smaller than the absorption grating. Indeed,

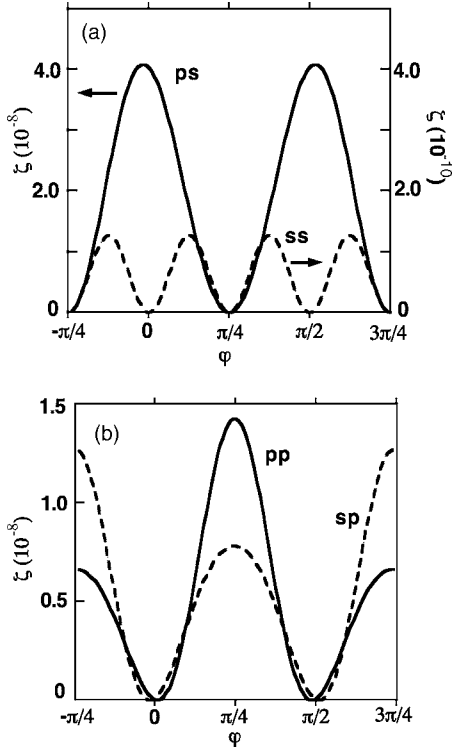


FIG. 2. (a) Calculated ζ as a function of azimuthal orientation angle φ for ps (solid curve) and ss (dashed) pump polarization pairs; (b) same as (a) but for pp polarization (solid curve) and sp polarization (dashed curve).

from the estimate of the pair grating amplitude above, one can also show that for typical injected carrier densities of 10^{17} cm^{-3} as used in the experiments, $\zeta < 5 \times 10^{-8}$ and so the pair gratings are very weak.

Figures 2(a) and 2(b) show theoretical values of the maximum ζ at 830 nm as a function of φ for the four different $\mu\nu$ and for $N_e^{inj} \sim 2 \times 10^{17} \text{ cm}^{-3}$, a typical density achieved in the experiments. The ss case yields the lowest calculated value, reflecting the relatively low amplitude pair grating produced by QUIC currents in this case. For the ps polarization case, the contribution to the grating amplitude from QUIC current generation is the same as for the ss case and the diffraction efficiency is dominated by the grating formed from the $\chi^{(2)}$ process. The simulations suggest that the ps case would yield the largest amplitude grating. The pp and sp polarization cases show contributions from, and interference between, the pair gratings formed from $\chi^{(2)}$ and QUIC current processes.

III. EXPERIMENTS

The material used for the experiments is an $L=790\text{-nm}$ -thick (001)-grown bulk GaAs sample and the measurements were performed at 300 K. For the ω pulses, we used 1550 nm pulses with a full width at half maximum (FWHM) of ~ 150 fs. These were produced by an optical parametric amplifier that is pumped by a regeneratively amplified Ti:sapphire laser operating at 250 kHz. The 2ω pulses with carrier wavelength of 775 nm and pulse width ~ 150 fs were produced by frequency doubling of the ω pulses in a

beta barium borate crystal. The ω and 2ω pump pulses were temporally and spatially overlapped on the sample with an angle of incidence of $\theta' = \pm 10^\circ$ from the normal (internal angle of $\theta \approx \theta'/n_{\omega,2\omega}$), resulting in $\Lambda_g = 2.2 \mu\text{m}$. The ω and 2ω pump beams had focal spot size (FWHM) of 60 and 110 μm , respectively. The sample is antireflection coated for 800 nm and so the internal and external intensities of the 775 nm beams were approximately the same. Incident intensities for the 1550 nm pulses were as high as 5 GW cm^{-2} , while those for the 775 nm pulse are less than 100 MW cm^{-2} . At the highest intensities, the pump pulses experienced some absorption saturation as discussed earlier.¹⁹ Given the 775 nm absorption depth of $\sim 0.7 \mu\text{m}$, there was a density and indeed a small current variation, with depth in the thin sample. Hence, all carrier density values quoted are estimated, depth-averaged values. A time-delayed s -polarized probe pulse with carrier wavelength of 830 nm and derived from the regenerative amplifier was focused at near-normal incidence to an $\sim 40 \mu\text{m}$ spot diameter within the pumping area, as shown in Fig. 1. The diffracted light was measured with a photomultiplier tube for various time delays from the pump pulses.

By also measuring the undiffracted transmission of the probe beam with (T') and without (T) one or both pump pulses present, we are also able to determine the differential transmission of the probe beam, $\Delta T/T = (T' - T)/T$. Under our pumping and probing conditions, theoretically one expects²⁷ $\Delta T/T \approx \alpha_{th} L f_e(E_{th})$.

IV. RESULTS AND DISCUSSION

Figures 3(a) and 3(b) show on different time scales the measured time dependence of ζ for incident $\sim 3 \text{ GW cm}^{-2}$ p -polarized 1550 nm and $\sim 100 \text{ MW cm}^{-2}$ s -polarized 775 nm pump pulses, each independently generating a peak carrier density¹⁹ of $\sim 1 \times 10^{17}$ and $\sim 3 \times 10^{17} \text{ cm}^{-3}$, respectively, when pump saturation effects are taken into account. From the discussion in Sec. II C, one would expect ζ to be dominated by a directly induced pair gratings (N_I^{ps} effect) with the current-induced pair grating amplitude N_J^{ps} being negligible. Also shown in Fig. 3(a) is the time-dependent $[\Delta T/T]^2$. Both $[\Delta T/T]^2$ and ζ are proportional to $(N_e^{inj})^2$. The initial fast rise approximately follows the square of the integral of the pump pulses but is also slowed and delayed slightly, since the pump pulses are coupled to conduction-band states with higher energy than that accessed by the probe pulse. Carrier thermalization and cooling of Γ -valley electrons therefore also influence the rise time of both $[\Delta T/T]^2$ and ζ during optical pumping. (Note that in the case where a current-induced population grating induces a pair grating, and therefore a carrier specific heat grating,¹⁹ as the semiconductor spatially uniformly absorbs energy from the pump pulses, a temperature grating also occurs. The decay of this temperature grating would produce a *decay* of the diffraction efficiency. For the directly deposited density grating with amplitude N_I^{ps} considered here, the optical energy deposition process is spatially periodic with the modulation in the carrier density or carrier specific heat having the same fractional amplitude as the energy deposition process itself.

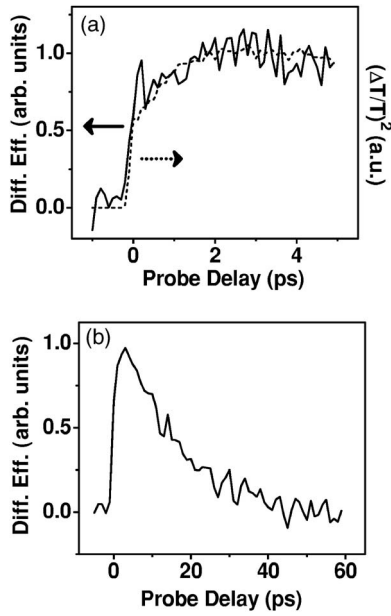


FIG. 3. (a) Measured diffraction efficiency ζ and square of differential probe transmission $[(\Delta T/T)^2]$ as a function of the time delay between the 830 nm probe pulse and 100 MW cm^{-2} *s*-polarized 775 nm and *p*-polarized 3 GW cm^{-2} 1550 nm pump pulses for $\varphi=0$. (b) Temporal dependence of ζ but for longer delays.

Therefore, no temperature grating forms.) After the initial rapid rise, both $[(\Delta T/T)^2]$ and ζ continue to increase on a time scale of a few picoseconds before beginning to decay through carrier recombination and diffusion, as shown in Fig. 3(b). This slowly rising component is likely due to the fact that the 1550 nm pulse, through free-carrier absorption, transfers electrons into *X* and *L* conduction-band valleys. These electrons, including a small number that help define an electron grating, are returned to the electron Γ valley²⁹ on a 2.5 ps time scale and increase the probe pulse transmission and diffraction.¹⁷ The returning electrons also bring $\sim 0.3 \text{ eV}$ of energy with them, which could also slow down the cooling rate of Γ -valley electrons.

From the direct pump-probe transmission studies, we measured the carrier recombination rate Γ to be $\sim .03 \text{ ps}^{-1}$, a not unexpected high rate because the sample is very thin and recombination is likely governed by surface defects.¹⁹ The decay rate for ζ is then $2[K_s^2 D_a + \Gamma]$, where D_a is the ambipolar diffusion constant. From the measured²¹ $D_a = 20 \text{ cm}^2 \text{ s}^{-1}$, one would expect a grating decay time of 12 ps, consistent with a value of $15 \pm 4 \text{ ps}$ obtained from the data.

For each of the four different polarization combinations $\mu\nu$, Fig. 4 shows the peak ζ as a function of angle φ for a probe delay of 3 ps and for pumping conditions corresponding to Fig. 3(a). For the *ps* combination, Fig. 4(a) shows data consistent with the $[\sin(2\varphi)]^2$ dependence predicted by Eq. (6). Within limitations of signal-to-noise ratio (S/N), there is no evidence of interference between directly deposited and current-induced pair gratings, consistent with the theoretical prediction that the latter is expected to be small. Figures 4(b)–4(d) show corresponding φ dependence of ζ for the *ss*,

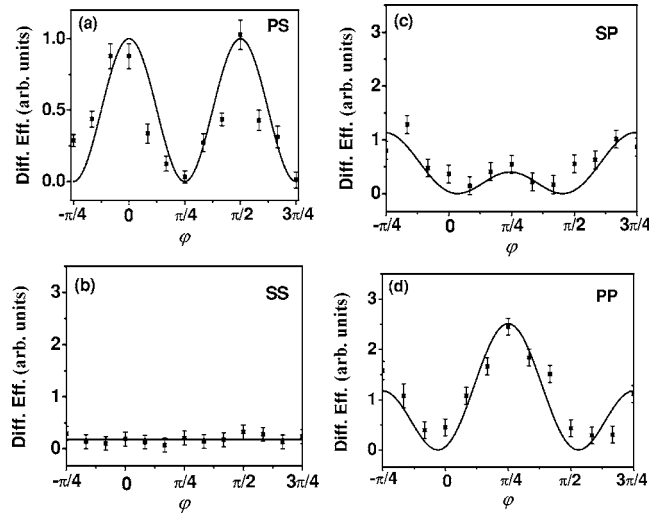


FIG. 4. Grating diffraction efficiency as a function of azimuthal angle φ for *ps*, *ss*, *pp*, and *sp* pump polarization combinations for pump intensities similar to that of Fig. 3.

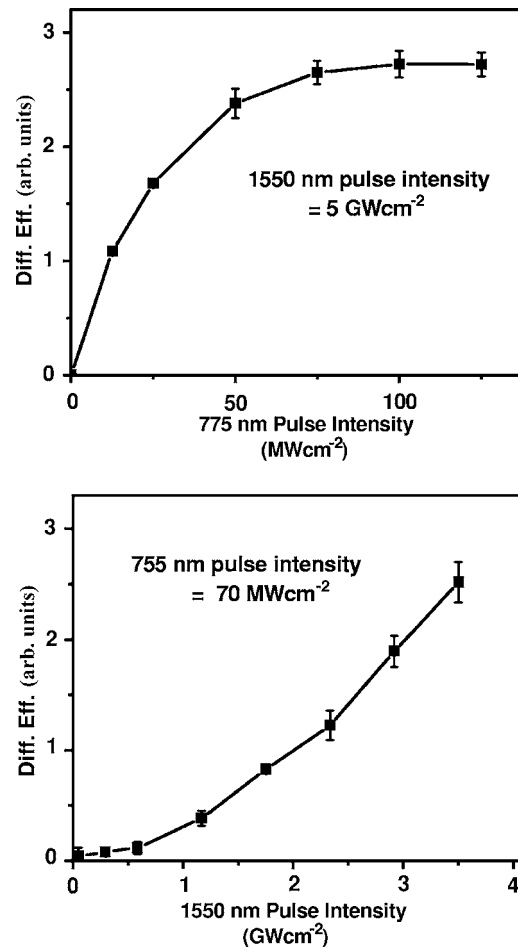


FIG. 5. Probe diffraction efficiency at 3 ps delay for $\varphi=0$ as a function of *s*-polarized 775 nm pulse intensity for *p*-polarized 1550 nm pulse intensity of 5 GW cm^{-2} ; (b) same as (a) except that it is now as a function of 1550 nm intensity for 775 nm intensity $= 70 \text{ MW cm}^{-2}$.

pp , and sp cases. Within S/N limitations, no grating is observed for the ss case, consistent with the theoretical discussion in Sec. II C and Fig. 2(a). The pp and sp cases, however, show superposition effects and interference between the two types of pair gratings and have an overall φ dependence consistent with that shown in Fig. 2(b). Interestingly, the ζ for pp and sp polarizations are peaked at angles φ that differ by π , as Fig. 2 also suggests. For a given polarization pair, from the difference in amplitude at the primary and secondary peaks, one can estimate that $N_j/N_l \approx 0.25$ in both cases, reasonably close to the theoretical estimated value of 0.5.

Finally, Fig. 5 shows how the diffraction efficiency of the directly deposited population grating generated by ps polarization varies with the intensity of one beam when the other beam intensity is held constant. For 3 ps delay and a fixed 1550 nm pulse intensity of 5 GW cm^{-2} , the diffraction efficiency varies linearly with the 775 nm intensity as expected from Eq. (6), but saturation is clearly observed beyond 30 MW cm^{-2} for which, assuming no saturation, the total peak carrier density would be $\sim 2 \times 10^{17} \text{ cm}^{-3}$. For our pump wavelengths, the density of electron states available to the 20 nm bandwidth pump pulses is $\sim 4 \times 10^{17} \text{ cm}^{-3}$. It is therefore not surprising that saturation effects become observable for $I^{2\omega} \sim 30 \text{ MW cm}^{-2}$. In Fig. 5(b), we show similar data for the diffraction efficiency as a function of 1550 nm pulse intensity for a constant 775 nm peak intensity of 70 MW cm^{-2} . At low intensities, a quadratic variation is observed, as expected, but the dependence approaches a linear behavior at high intensities. For a 1550 nm beam intensity of 3 GW cm^{-2} , the estimated total peak carrier density is 2

$\times 10^{17} \text{ cm}^{-3}$, and therefore it is not surprising that saturation effects should become observable.

V. CONCLUSIONS

We have investigated the generation of electron-hole pair density gratings formed by the quantum interference of absorption pathways for 1550 and 775 nm pulses when the two pulses are noncollinearly incident on a GaAs sample at 300 K. Transient pair gratings can be generated in two different ways. One is associated with a $\chi^{(2)}$ optical nonlinearity and leads to a directly deposited pair grating. The other pair grating is generated following the dielectric relaxation of electron and hole charge population gratings following charge current injection via a $\chi^{(3)}$ nonlinearity. We have studied the two grating types as a function of pump beam polarization and sample orientation. Interestingly, in cases where both grating types simultaneously exist, they are comparable in amplitude. As a result, they superpose, leading to interference effects.

ACKNOWLEDGMENTS

This work was supported in part by the Natural Sciences and Engineering Research Council of Canada, Photonics Research Ontario, the Defence Advanced Research Projects Agency, and the Office of Naval Research. The authors gratefully acknowledge stimulating discussions with Phil Marsden, Ali Najmaie, and John E. Sipe.

*Electronic address: vandriel@physics.utoronto.ca

¹B. I. Sturman and V. M. Fridkin, *The Photovoltaic and Photorefractive Effects in Noncentrosymmetric Materials* (Gordon and Breach, Philadelphia, 1992).

²E. Dupont, P. B. Corkum, H. C. Liu, M. Buchanan, and Z. R. Wasilewski, *Phys. Rev. Lett.* **74**, 3596 (1995).

³R. Atanasov, A. Haché, J. L. P. Hughes, H. M. van Driel, and J. E. Sipe, *Phys. Rev. Lett.* **76**, 1703 (1996); A. Hache, Y. Kostoulas, R. Atanasov, J. L. P. Hughes, J. E. Sipe, and H. M. van Driel, *ibid.* **78**, 306 (1997). H. M. van Driel and J. E. Sipe, in *Ultrafast Phenomena in Semiconductors*, edited by K.-T. Tsen (Springer-Verlag, New York, 2001), p. 261.

⁴M. Sheik-Bahae, *Phys. Rev. B* **60**, R11257 (1999).

⁵S. D. Ganichev, E. L. Ivchenko, V. V. Bel'kov, S. A. Tarasenko, M. Sollinger, D. Weiss, W. Wegscheider, and W. Prettl, *Nature (London)* **417**, 153 (2002).

⁶R. D. R. Bhat and J. E. Sipe, *Phys. Rev. Lett.* **85**, 5432 (2000).

⁷M. J. Stevens, A. L. Smirl, R. D. R. Bhat, A. Najmaie, J. E. Sipe, and H. M. van Driel, *Phys. Rev. Lett.* **90**, 136603 (2003); J. Hubner, W. W. Rühle, M. Klude, D. Hommel, R. D. R. Bhat, J. E. Sipe, and H. M. van Driel, *ibid.* **90**, 216601 (2003).

⁸D. H. Marti, M. A. Dupertuis, and B. Deveaud, *Phys. Rev. B* **69**, 035335 (2004); **72**, 075357 (2005).

⁹R. D. R. Bhat, F. Nastos, A. Najmaie, and J. E. Sipe, *Phys. Rev. Lett.* **94**, 096603 (2005).

¹⁰H. Zhao, X. Pan, A. L. Smirl, R. D. R. Bhat, A. Najmaie, J. E. Sipe, and H. M. van Driel, *Phys. Rev. B* **72**, 201302(R) (2005).

¹¹H. T. Duc, T. Meier, and S. W. Koch, *Phys. Rev. Lett.* **95**, 086606 (2005).

¹²N. Laman, A. Shkrebti, J. Sipe, and H. van Driel, *Appl. Phys. Lett.* **75**, 2581 (1999).

¹³M. Stevens, A. Smirl, R. Bhat, J. Sipe, and H. van Driel, *J. Appl. Phys.* **91**, 4382 (2002).

¹⁴V. V. Bel'kov, S. D. Ganichev, P. Schneider, C. Back, M. Oestreich, J. Rudolph, D. Hägele, L. E. Golub, W. Wegscheider, and W. Prettl, *Solid State Commun.* **128**, 283 (2003).

¹⁵M. Bieler, N. Laman, H. M. van Driel, and A. L. Smirl, *Appl. Phys. Lett.* **86**, 061102 (2005).

¹⁶J. M. Fraser, A. J. Shkrebti, J. E. Sipe, and H. M. van Driel, *Phys. Rev. Lett.* **83**, 4192 (1999); J. M. Fraser and H. M. van Driel, *Phys. Rev. B* **68**, 085208 (2003).

¹⁷M. J. Stevens, R. D. R. Bhat, X. Y. Pan, H. M. van Driel, and A. L. Smirl, *J. Appl. Phys.* **97**, 093709 (2005).

¹⁸Y. Kerachian, P. Nemeč, H. van Driel, and A. Smirl, *J. Appl. Phys.* **96**, 430 (2004).

¹⁹Y. Kerachian, P. A. Marsden, H. M. van Driel, and A. L. Smirl, preceding paper, *Phys. Rev. B* **75**, 125205 (2007).

²⁰O. Madelung, *Semiconductors: Basic Data* (Springer, Berlin, 1996).

²¹J. S. Blakemore, *J. Appl. Phys.* **53**, R123 (1982).

- ²²M. D. Dvorak, W. A. Schroeder, D. R. Andersen, A. L. Smirl, and B. S. Wherrett, *IEEE J. Quantum Electron.* **30**, 256 (1994); D. C. Hutchings and B. S. Wherrett, *Phys. Rev. B* **49**, 2418 (1994).
- ²³R. D. R. Bhat and J. E. Sipe, *Phys. Rev. B* **72**, 075205 (2005).
- ²⁴R. D. R. Bhat and J. E. Sipe (unpublished).
- ²⁵A. Haché, J. E. Sipe, and H. M. van Driel, *IEEE J. Quantum Electron.* **34**, 1144 (1998).
- ²⁶P. Langot, R. Tommasi, and F. Vallée, *Phys. Rev. B* **54**, 1775 (1996).
- ²⁷B. A. Bennet, R. A. Soref, and J. A. Del Alamo, *IEEE J. Quantum Electron.* **26**, 113 (1990).
- ²⁸A. Yariv and P. Yeh, *Optical Waves in Crystals* (Wiley, New York, 1984).
- ²⁹J. Shah, B. Deveaud, T. C. Damen, W. T. Tsang, A. C. Gossard, and P. Lugli, *Phys. Rev. Lett.* **59**, 2222 (1987); S. Zollner, S. Goplan, and M. Cardona, *J. Appl. Phys.* **68**, 1682 (1990); D. Y. Oberli, J. Shah, and T. C. Damen, *Phys. Rev. B* **40**, 1323 (1989).